PNAS
www.pnas.org

Supplementary Information for

CRY2 isoform selectivity of a circadian clock modulator with anti-glioblastoma efficacy

Simon Miller[a], Manish Kesherwani[a], Priscilla Chan[b], Yoshiko Nagai[a], Moeri Yagi[a,c], Jamie Cope[d], Florence Tama[a,e,f], Steve A. Kay[b,*], and Tsuyoshi Hirota[a,c,*]

[a]Institute of Transformative Bio-Molecules, Nagoya University, Nagoya 464-8601, Japan
[b]Keck School of Medicine, University of Southern California, Los Angeles, CA 90089, USA
[c]Division of Biological Sciences, Graduate School of Science, Nagoya University, Nagoya 464-8601, Japan
[d]Synchronicity Pharma, Inc. 1416 Saratoga Avenue #133, San Jose, CA 95129, USA
[e]Department of Physics, Graduate School of Science, Nagoya University, Nagoya 464-8601, Japan
[f]RIKEN-Center for Computational Science, Kobe 650-0047, Japan

*Steve A. Kay
Email: stevekay@usc.edu

*Tsuyoshi Hirota
Email: thirota@itbm.nagoya-u.ac.jp

This PDF file includes:

Figures S1 to S6
Tables S1 to S2

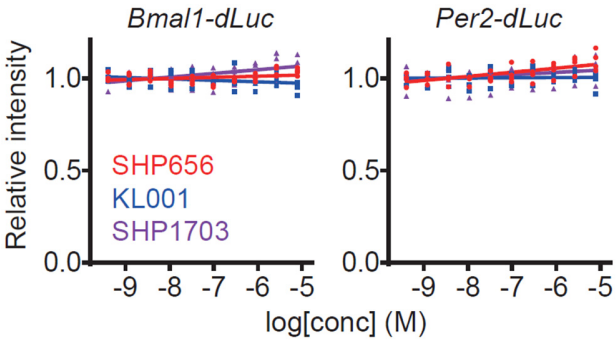

Fig. S1. Effects of KL001, SHP656, and SHP1703 on cell viability. Cellular ATP levels after treatment of *Bmal1-dLuc* and *Per2-dLuc* U2OS cells with various concentrations of compounds are plotted by setting a DMSO control to 1 (n = 4 biologically independent samples).

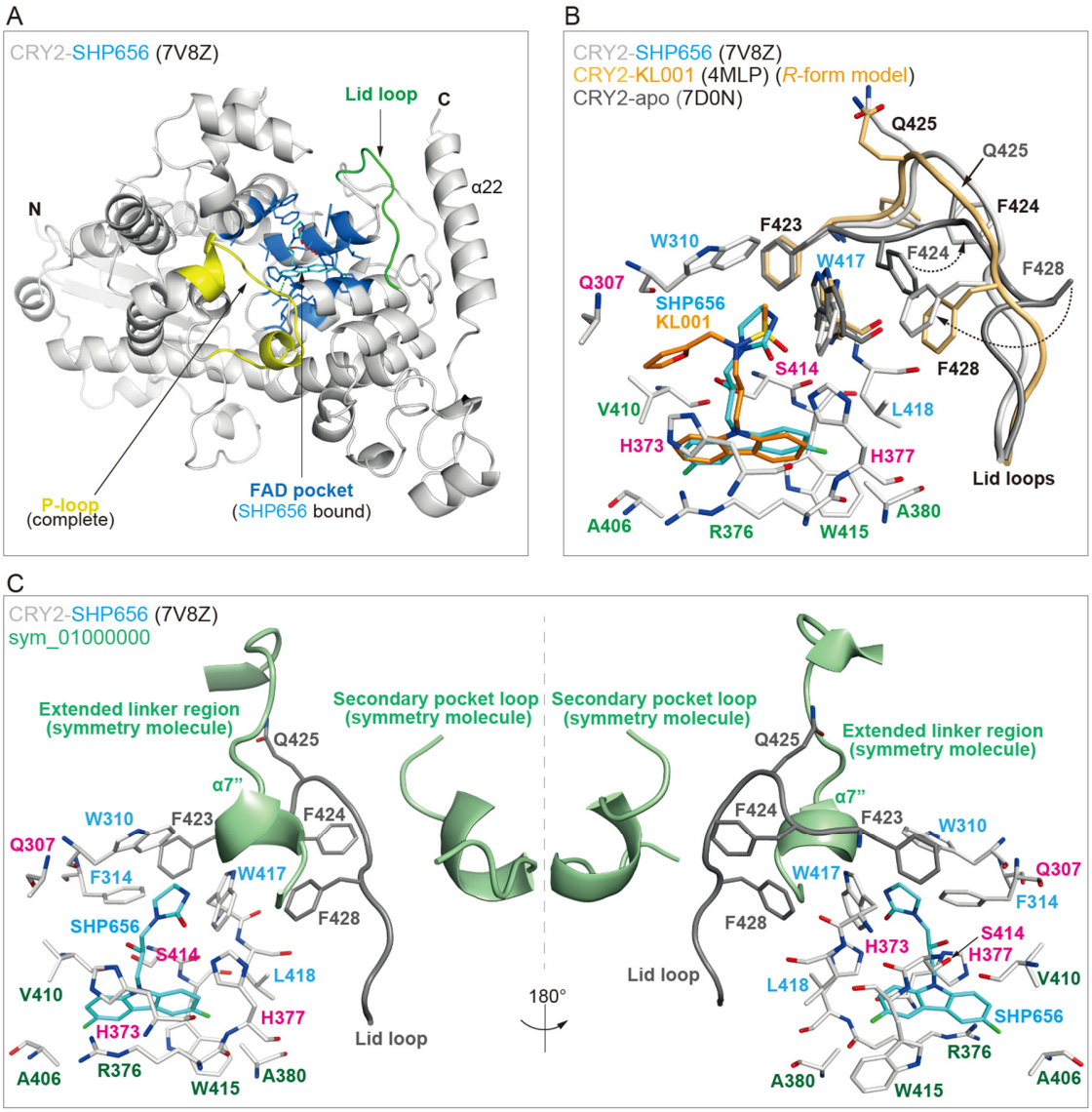

Fig. S2. Crystal structure of CRY2-SHP656. (A) The overall structure of CRY2-SHP656 (PDB ID: 7V8Z). Key structural and regulatory elements include the FAD pocket (blue), lid loop (green), and the P-loop (yellow). (B) Superposition of CRY2-KL001 (light orange-orange) and CRY2-apo (gray) onto CRY2-SHP656 (white-cyan). F428 in the lid loop rotated ~180° in CRY2-SHP656 compared to CRY2-apo, and was positioned closer to the FAD pocket with respect to CRY2-KL001. (C) Crystal packing around the lid loop of CRY2-SHP656 (white-cyan). A symmetry-related molecule (green) was in close proximity to the lid loop (gray). The right panel shows a 180° rotated view around the Y-axis with respect to the left panel.

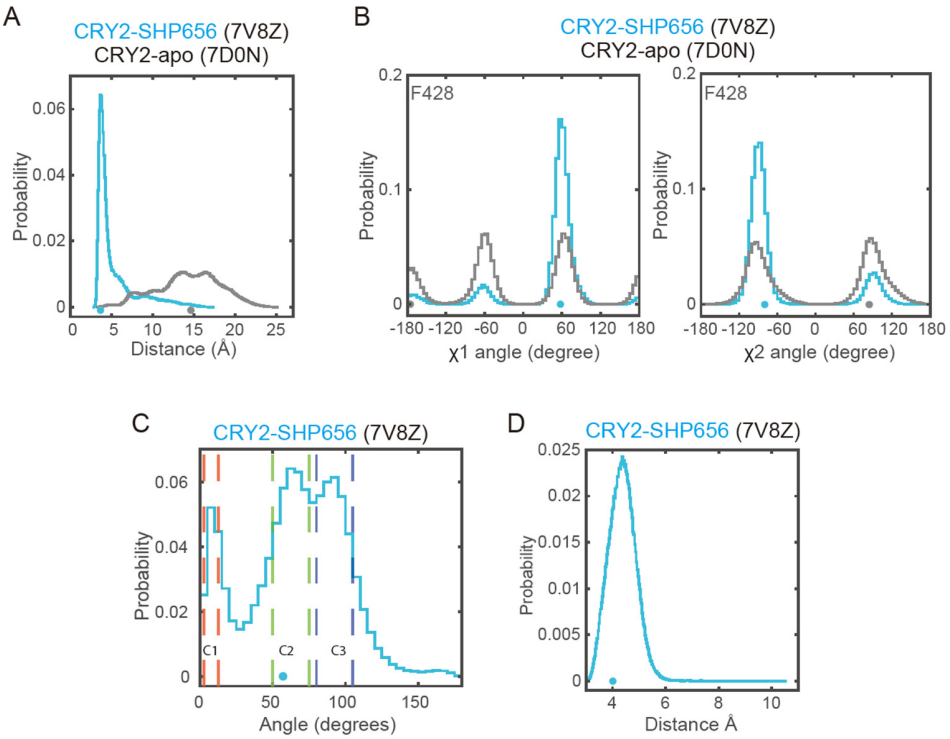

Fig. S3. MD simulation of CRY2-SHP656. (A) Stable interaction between the gatekeeper W417 and F428. In MD simulations, F428 maintained close proximity to the gatekeeper W417 in CRY2-SHP656 (cyan), but was too distant to form a stacking interaction in CRY2-apo (gray). The colored dots represent the distance between W417 and F428 in the crystal structures. The side chain of F428 was truncated in the CRY2-apo crystal structure and was modeled for the simulation. (B) F428 was stable in CRY2-SHP656. The χ1 and χ2 angles showed less variation in an MD simulation of CRY2-SHP656 (blue) compared to CRY2-apo (gray). The colored dots represent the χ angles observed in the crystal structures. (C) 2-imidazolidinone orientations during MD simulation. Two major populations of 2-imidazolidinone position were observed, clusters C2 and C3, and one minor orientation C1. C2 showed slight predominance and most closely represented the orientation in the CRY2-SHP656 crystal structure (shown as a blue dot). (D) The Gatekeeper maintained a constant interaction with the 2-imidazolidinone of SHP656. The distance between the gatekeeper and 2-imidazolidinone was consistent among C1-C3 orientations. The blue dot represents the distance observed in the CRY2-SHP656 crystal structure.

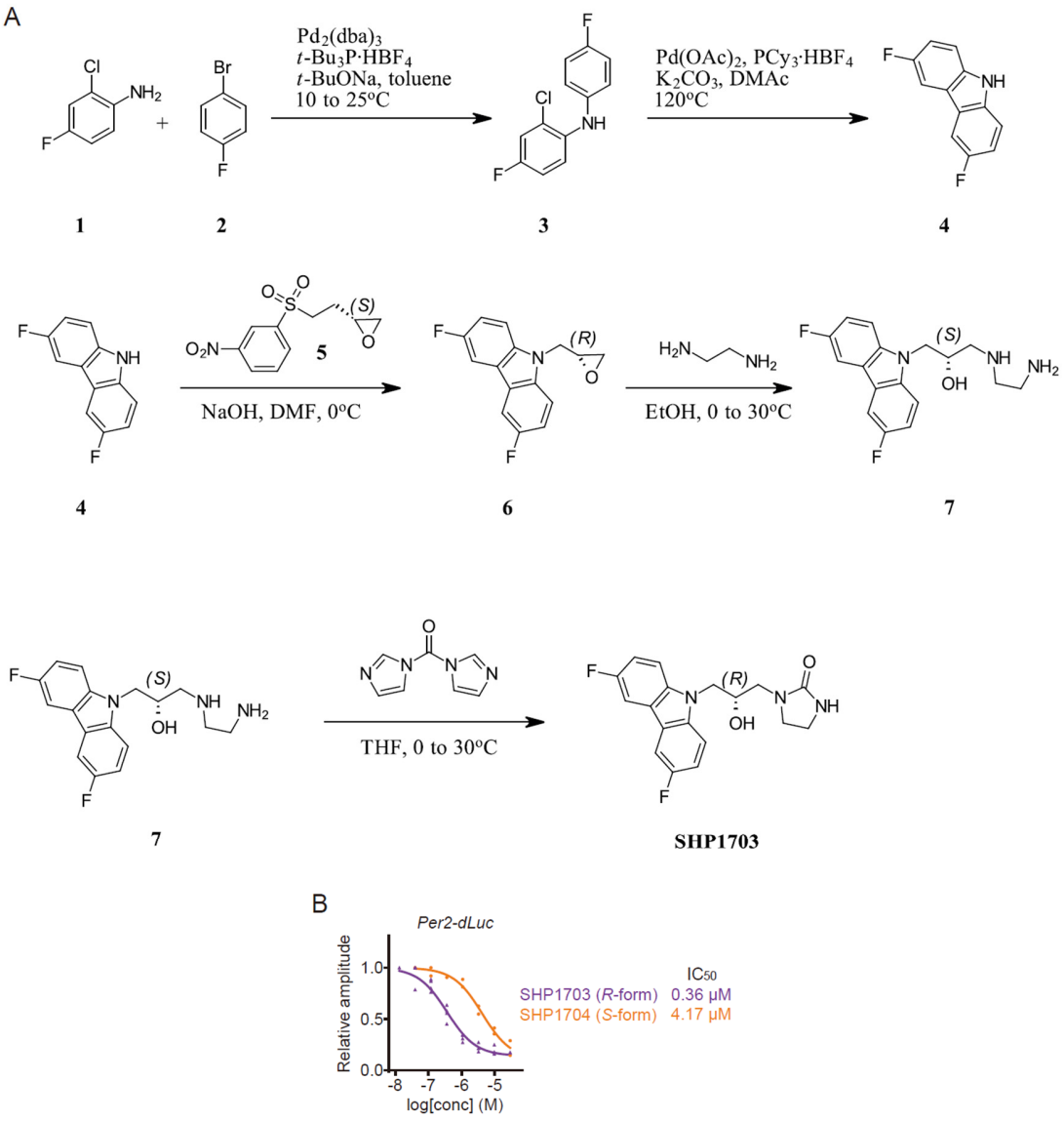

Fig. S4. (A) Synthesis of SHP1703 (pure *R*-form of SHP656). (B) Effects of SHP1703 and SHP1704 (pure *R*-form and *S*-form of SHP656, respectively) on *Per2-dLuc* in U2OS cells. Changes in circadian amplitude compared to a DMSO control are shown (n = 2-4 biologically independent samples). Concentrations for 50% inhibition (IC_{50}) are indicated.

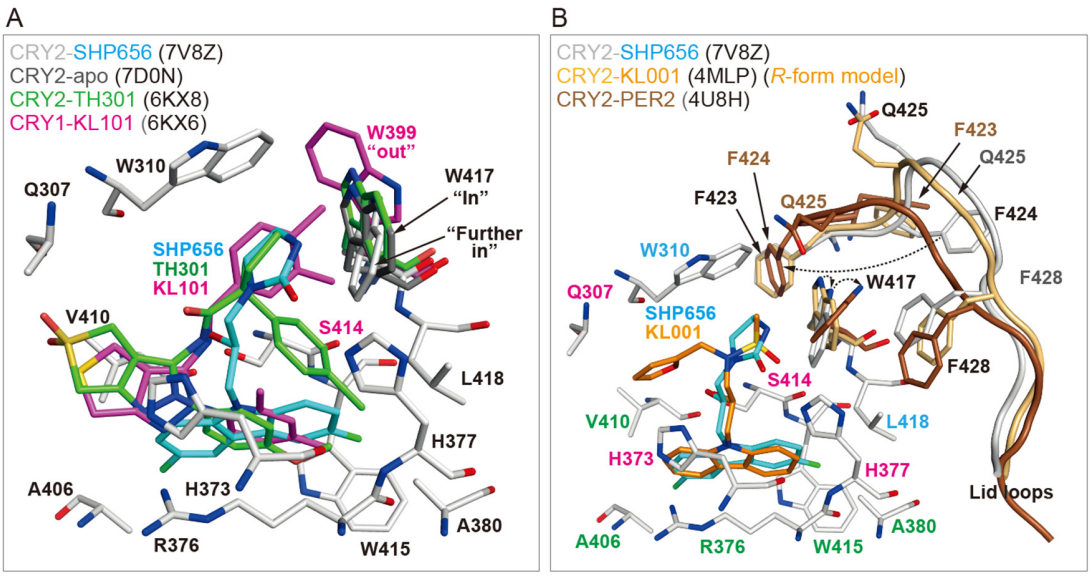

Fig. S5. Comparison of CRY2 and CRY1 structures. (A) The gatekeeper tryptophan is differentially arranged upon the binding of CRY isoform-selective compounds. Superposition of CRY2-apo (gray), CRY2-TH301 (green) and CRY1-KL101 (magenta) onto CRY2-SHP656 (white-cyan). The steric bulk of the dimethylphenyl of KL101 requires an "out" gatekeeper, which is intrinsic to CRY1. The binding of TH301 to CRY2 did not induce a conformational change in the gatekeeper, compared to CRY2-apo. CRY2-SHP656 had a "further in" conformation that was different to other structures. The 2-imidazolidinone group of SHP656 has similar steric bulk to the cyclopentyl of TH301, although the orientation of the five-membered ring was slightly rotated. (B) Gatekeeper and lid loop conformations upon ligand and PER binding. Superposition of CRY2-KL001 (light orange-orange) and CRY2-PER2 (brown) onto CRY2-SHP656 (white-cyan). Complex formation between CRY2 and PER2 induced a conformational change in the N-terminal portion of the lid loop. F423 and F424 swapped positions (long, dashed arrow) where F424 inserted into the auxiliary pocket, different from other CRY2 structures. F428 in all three structures was positioned adjacent to the gatekeeper, albeit with slightly offset positions. The gatekeeper adopted "in", "further in" and "middle" conformations in CRY2-SHP656, CRY2-KL001 and CRY2-PER2, respectively.

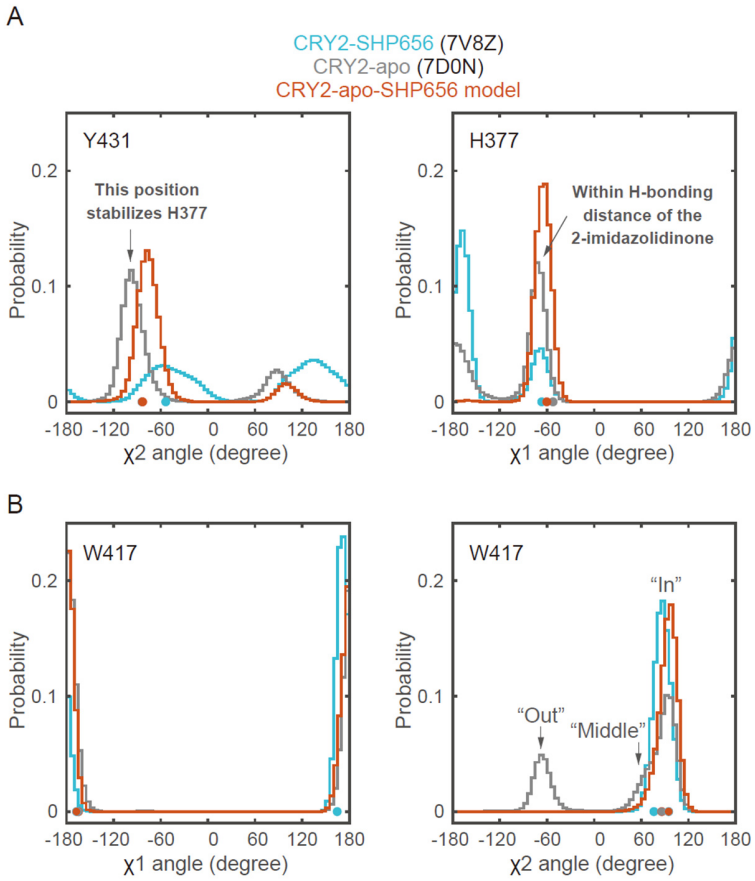

Fig. S6. A lid loop disulfide bond affects residue flexibility in MD simulations. (A) The χ2 angles of Y431 (left panel) in the disulfide bond-containing CRY2-SHP656 structure (blue) and no disulfide bond-containing CRY2-apo (gray), correlate to different flexibility and χ1 angles observed for H377 (right panel). CRY2-apo-SHP656 model (orange) is also shown. The colored dots represent the χ1 and χ2 angles observed in the crystal structures of CRY2-SHP656 (blue) and CRY2-apo (gray), and the minimized structure of the CRY2-apo-SHP656 model (orange). (B) Gatekeeper W417 χ1 and χ2 angles in CRY2-apo-SHP656 model MD simulations. Data for CRY2-SHP656 (blue) and CRY2-apo (gray) are replicated from Fig. 3C for comparison.

Table S1. Data collection and refinement statistics.

	CRY2-SHP656 (7V8Z)	**CRY2-SHP1703 (7V8Y)**
Data collection		
Space group	$P6_5$	$P6_5$
Cell dimensions		
a, b, c (Å)	77.7, 77.7, 159.2	77.7, 77.7, 159.2
α, β, γ (˚)	90, 90, 120	90, 90, 120
Resolution (Å)	1.95 (2.06-1.95)	1.90 (2.0-1.9)
R_{merge}	0.082 (0.512)	0.060 (0.496)
$I/\sigma(I)$	21.7 (6.1)	29.1 (6.0)
$CC_{1/2}$	0.999 (0.968)	1.0 (0.971)
Completeness (%)	100 (100)	99.9 (99.2)
Redundancy	17.0 (16.9)	20.4 (19.9)
Refinement		
Resolution (Å)	51.4-1.95	38.9-1.9
No. reflections unique	672686, 39503	865991, 42509
R_{work}/R_{free} (%)	0.172/0.190	0.167/0.183
No. atoms	4071	4111
Protein	3820	3821
Ligand/ion	25	25
Water	226	265
R.m.s. deviations		
Bond lengths (Å)	0.006	0.010
Bond angles (˚)	0.78	1.00
Ramachandran		
Favored (%)	97.53	97.74
Allowed (%)	2.47	2.26
Outliers (%)	0	0
Average B-factors		
Protein	34.4	34.9
Ligand	26.6	28.7
Solvent	38.4	40.7

Values in parentheses are for the highest resolution shell.

Table S2. Statistical analysis of Fig. 4F.

	SHP1703	SHP1704
100 μM		
IMR-90 vs. MGG 31	ns	ns
IMR-90 vs. MGG 31 DGC	****	*
MGG 31 vs. MGG 31 DGC	****	*
50 μM		
IMR-90 vs. MGG 31	***	ns
IMR-90 vs. MGG 31 DGC	ns	****
MGG 31 vs. MGG 31 DGC	*	****
25 μM		
IMR-90 vs. MGG 31	***	ns
IMR-90 vs. MGG 31 DGC	**	ns
MGG 31 vs. MGG 31 DGC	ns	ns
12.5 μM		
IMR-90 vs. MGG 31	****	ns
IMR-90 vs. MGG 31 DGC	****	**
MGG 31 vs. MGG 31 DGC	ns	***
6.25 μM		
IMR-90 vs. MGG 31	**	ns
IMR-90 vs. MGG 31 DGC	****	ns
MGG 31 vs. MGG 31 DGC	ns	ns
3.0 μM		
IMR-90 vs. MGG 31	ns	ns
IMR-90 vs. MGG 31 DGC	ns	ns
MGG 31 vs. MGG 31 DGC	ns	ns
1.5 μM		
IMR-90 vs. MGG 31	ns	ns
IMR-90 vs. MGG 31 DGC	ns	ns
MGG 31 vs. MGG 31 DGC	ns	ns
0.75 μM		
IMR-90 vs. MGG 31	ns	ns
IMR-90 vs. MGG 31 DGC	ns	ns
MGG 31 vs. MGG 31 DGC	ns	ns
0.375 μM		
IMR-90 vs. MGG 31	ns	ns
IMR-90 vs. MGG 31 DGC	ns	ns
MGG 31 vs. MGG 31 DGC	ns	ns

****P < 0.0001; ***P < 0.001; **P < 0.01, *P < 0.05 by two-way ANOVA followed by Tukey's multiple comparisons test. ns, not significant.